Journal of
Engineering Sciences
Faculty of Engineering
Assiut University
JES
مجلة
العلوم الهندسية
كلية الهندسة
جامعة أسيوط
journal homepage: http://jesaun.journals.ekb.eg

Evaluation of the Applications of using Global free Digital Elevation Models and GNSS-RTK data for Agricultural purposes in Egypt using Machine Learning

Received 8 October 2024; Revised 25 November 2024; Accepted 25 November 2024

Ashraf ABDALLAH [1]
Bara' Al-MISTAREHI [2]
Amir SHTAYAT [3]

Keywords
DEM; GNSS-RTK; Agricultural; Machine Learning; Egypt

Abstract: Agriculture is a vital component of Egypt's economy; therefore, using Digital Elevation Models (DEMs) in agricultural planning in Egypt has significant benefits regarding water management, site appropriateness assessment, flood risk mitigation, and infrastructure construction. It is also essential for planners to make more informed decisions, optimize resource allocation, and support sustainable farming practices. This research paper investigates the accuracy of obtaining DEM data from four free global models (STRM30, ALOS30, COP30, and TanDEM-X90). The global DEM data has been compared to an actual GNSS-RTK DEM data surveyed onsite for two agricultural block areas in Aswan, the southern Government of Egypt. The two blocks are a part of a national project. For Block I and II, the RMSE of the Model STRM30 was 2.92 m and 3.59 m, respectively, indicating a poorer solution. Regarding accuracy, the ALOS30 model ranks third, reporting an RMSE of 2.58 m for block II and 3.30 m for block I. COP30 has an RMSE value of 1.06 m for blocks I and II and.91 m overall. TanDEM-X90 is the most accurate model in this investigation; block I provided an RMSE of 0.90 m with an SD of 0.58 m ($SD_{95\%}$ = 0.38 m). After removing the anomalies, the model's stated RMSE for block II was 0.34 m, with an SD value of 0.62 m and 1.03 m. According to the classification using machine learning algorithms, with an accuracy of 84.7% for block I and 85% for block II, TanDEM-X90 is the best solution.

1. Introduction

Digital elevation models (DEMs) are crucial inputs for environmental and landscape modelling and spatial analysis. These models provide topographic and terrain characteristics, including slope aspect, slope, channels, and hillslopes [1], especially for

[1] Faculty of Engineering, Aswan University, Aswan, Egypt
[2] Department of Civil Engineering, Jordan University of Science and Technology, Irbid, Jordan
[3]Department of City Planning and Design, Jordan University of Science and Technology, Irbid 22110, Jordan

https://doi.org/10.21608/jesaun.2024.326709.1374

geomorphology studies [2], geology [3], hydrology [4], and Civil Engineering [5]. Modelling to prevent natural disasters is one of its applications (floods [6], soil erosion Studies [7], weather forecasting [8], and climate change [9]). Digital Surface Model (DSM), Digital Terrain Model (DTM), and (DEM) can all sound like they mean different things. The word "DSM" means a specific type of DEM, where the elevations cover the buildings, plants, and other things on Earth's surface [10]. The term "DTM" refers to a model that shows the heights of bare ground. DEM is a broad word that can mean either of these things. It is important to remember that a DEM is a subset of a DTM, even though the names don't mean the same thing. For this reason, a DTM can show more anatomical details. [11].

One must have a coordinate system and a reference frame to make use of a DEM. The metadata has to indicate the horizontal, vertical, and temporal elements among the data components. Datums are set across several historical eras and at varying global, regional, national, or local sizes. Choosing a horizontal datum—often WGS84 or a related standard—determines how longitude and latitude coordinates relate to the surface of the Earth. Based on either an ellipsoidal or geoidal (mean sea level) frame of reference, the vertical datum sets the reference point for elevations. Like EGM2008, global geoidal datums [12] and EGM96 [13] are possible. Figure 1 shows the relations between ellipsoidal height (h), orthometric height (H), and geoid undulation (N). The ellipsoidal height is estimated using equation (1) [14].

$$\eta = H + N \tag{1}$$

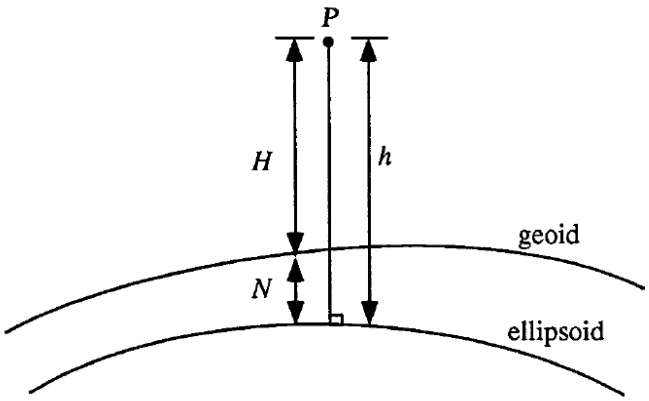

Figure 1: Orthometric versus ellipsoidal heights [14]

Various surveying techniques are used to create the (DEM). [15] compared the DEM created by Total station and those using post-processing kinematic single frequency GPS data. [16] studied the efficiency of the GNSS-PPP solution [17] and in comparison to the GNSS differential solution [18]. The study showed that the Root Mean Square Error (RMSE) was 2-3 cm between the differential and PPP solution. In addition to the classical survey, DEM is established through various methods, including airborne or satellite-borne

stereoscopic photogrammetry, interferometry of RADAR or SAR, and airborne laser scanning. Each technique's limitations depend on cost, precision, sample density, and preprocessing prerequisites. Typically, a DEM-generated procedure comprises five steps: data acquisition, resampling of grid spacing, height interpolation, repetition, and accuracy evaluation [19]. [20] explained that the error of the DEM is associated with grid spacing and interpolating techniques as well as resampling methods. These errors on a DEM spatial scale have been categorized as gross errors resulting from data collection, systematic errors arising from the establishment of elevation height values in the stereo image, and random errors arising from unknown sources. The variability of their defects across different terrains is due to topographical conditions [21]. Nowadays, different open-source Global DEMs are downloadable free of charge from the official provider's websites, such as the Shuttle Radar Topography Mission (SRTM) [22], and [23], ALOS Global Digital Surface Model (AW3D30) [24], and TanDEM-X [25].

Many researchers investigated the accuracy of such free DEMs in various disciplines. [26] assessed the effectiveness of AW3D30, TanDEM-X, and SRTM- across four distinct geographical regions characterized by diverse topography and land cover conditions. The study adjusted the resolution of the global models to match a reference model resolution of 1 m. It then assessed the accuracy by creating error rosters and producing descriptive statistics. The study found that slope had the most significant impact on the accuracy of the (DEM), with AW3D30 exhibiting the highest level of durability and stability. In addition, SRTM showed a slight improvement; moreover, TanDEM-X performed the worst in all case studies. [27] assessed the precision of (DEM) products across different topography and land cover regions and features. It focused on a specific case study conducted on Shikoku Island, Japan. The generated data exhibited errors in the topography and land cover classification. The study assessed six open-source (DEMs) and their characteristics in Shikoku Island, Japan, by comparing them to reference elevation points obtained through GPS observations. The terrain's characteristics have been observed to be influenced by the error of (DEMs). Based on the root mean square error (RMSE), the accuracy values of high-resolution (DEMs) are 9.9 m and 10.1 m for ASTER and SRTM, individually. [٢٨] conducted an initial assessment of the accuracy of TanDEM-X for specific floodplain locations and compared it to the SRTM model's widely used global (DEMs). The findings indicate that TanDEM-X demonstrates comparable average vertical accuracy, which is a significant improvement over the SRTM model. As well, an analysis was conducted to assess the vertical accuracy of land cover. The results suggest that the TanDEM-X model is the most precise global (DEM) across all land cover categories.

The accuracy of elevation data acquired from six main publicly available satellite-derived DEMs was analysed by [29]. The study also examined the extent to which accuracy can be enhanced by employing a correction method (linear fit) with Differential Global Positioning System (DGPS) estimates at Ground Control Points (GCPs). The studied location is characterised by a rugged granite terrain that is primarily flat but also includes undulating

and uneven surfaces. Furthermore, the study investigated the influence of resampling techniques and identified the optimal number of ground control points (GCPs) to reduce errors in future applications. The systematic error is eliminated by utilising DGPS data at GCPs, which significantly reduces bias. Consequently, it is recommended that DEMs be corrected using DGPS before their use in scientific research.

The accuracy of SRTM30 and AW3D30 models was compared to that of 117 GCPs in a study of the topography of 3837 km^2 in the Lower Tapi Basin, India. The RMS error of the DEM obtained for the SRTM and AW3D30 models was 2.88 m and 2.45 m, respectively [30]. The accuracy of the original TanDEM-X DEM and its enhanced edited variant, the Copernicus DEM, was assessed in [31] across three prominent mountain ranges in Europe: the Alps, the Carpathians, and the Pyrenees. The evaluation used a standard digital surface model derived from airborne laser scanning data. Furthermore, it assessed the suitability of terrain attributes (slope, aspect, and altitude) and data acquisition characteristics (coverage map, consistency mask, and height error map) for locating problematic sites. They have demonstrated that the Copernicus DEM at 30 m and 90 m resolutions represent the Earth's surface with greater precision than the TanDEM-X-90 and SRTM DEMs. [32] investigated the STRM model's accuracy for areas with moderate, intermediate, and steep slopes. In the region with a moderate slope, the SRTM model's vertical accuracy was determined to be 11.899 meters. The investigation discovered that the solution had an accuracy of 40.538 m for steep slopes and 21.609 m for areas with moderate slopes. More results for different models are explained in [33], [34], and [35].

Agriculture is essential to Egypt's economy, providing job opportunities and guaranteeing food security for its rising population. DEMs are particularly important in Egypt's agriculture, as topography influences water management, soil fertility, and crop compatibility. This motivation statement intends to emphasize the motivations for investigating DEMs and their use in agricultural practices in Egypt. The following points highlight the importance of the DEM model in agriculture. Sustainable agriculture in Egypt requires effective water management due to limited water resources. DEMs offer detailed information about topography and terrain features, making it possible to identify and map watersheds, drainage patterns, and potential water storage areas. Researchers and water resource managers can use DEMs to improve irrigation planning, implement precision water application techniques, and develop effective water conservation and allocation strategies. Precision farming and crop compatibility: To find out which crops will grow well together and use precision farming methods, it's important to know how the land's features and changes affect farming areas. DEMs give elevation information, which can be combined with other geographical details like soil type, sun exposure, and slope to figure out which areas are best for growing certain foods. When farmers learn about DEMs, they can make better decisions about which crops to grow, how to put them, and how much fertilizer to use. This leads to higher yields and better use of resources. Effective land use planning aims to facilitate sustainable growth and optimize agricultural capacity. DEMs

encompass crucial data about the heights of land, the shapes of landforms, and the differences in land cover. This data aids Egypt in optimizing the utilization of land resources, attaining harmonious urban-rural development, and fostering agricultural growth.

This research paper aims to investigate the following objectives:

- To assess the suitability of the open-source DEM models (SRTM, AW3D30 (ALOS30), COP30 and TanDEM-X) in comparison to the GNSS-RTK solution.
- To use the acquired DEM solution for agricultural planning in Egypt, which offers significant advantages in terms of infrastructure construction, water management, site suitability assessment, soil conservation, and flood risk reduction.
- To investigate DEMs, optimize resource allocation, and promote sustainable farming practices to assist planners in making better judgments.
- To integrate DEMs with other geospatial data to improve agricultural production, resilience, and long-term development in Egypt's farming industry.

The paper contains six chapters, the first of which is the introduction. The second chapter describes the four types of DEMs utilized in the evaluation, as well as the GNSS solution principles. The third chapter describes the methodology utilized in the processing. The fourth chapter compares the findings of each DEM model with the GNSS-RTK solution. The fifth chapter explains the fundamentals of machine learning and its results. The final chapter concludes the findings.

2. Materials and Methods

2.1. GNSS Solution

Using multiple GNSS constellations for positioning improves accuracy, dilution of precision (DOP), availability, and reliability [36]. Currently, there are four GNSS operating systems: NAVSTAR GPS (American), GLONASS (Russian), Galileo (European), and BeiDou (Chinese). However, until 2019, only GPS and GLONASS have been operational. Relative positioning, sometimes called differential Global Navigation Satellite Systems (DGNSS), is one technique for attaining centimetre-level positional precision. DGNSS uses a fixed, known position ground reference station (base station) to increase positioning accuracy. The rover, the second GNSS receiver, has two modes of operation: kinematic and static. Both receivers need to watch the identical satellites simultaneously. Since the errors affecting the base and rover's observations are similar, it is possible to estimate the baseline between them [18]. More details about the technique of GNSS can be seen in [14], [18], and [17].

2.2. SRTM3-30 DEM

The Shuttle Radar Topography Mission (SRTM) was a joint project of the National Aeronautics and Space Administration (NASA), the National Geospatial-Intelligence

Agency (NGA), the German Space Agency (DLR), and the Italian Space Agency (ASI). This global project started in February 2000 [37]. First, the United States Geological Survey (USGS) released a global C-band DEM version in 2003 with a spatial resolution of 90 m (3 arcsec). The first almost worldwide high-resolution DEM produced was this one. [38]. Later, SRTM2 (version 2) was created, which included several improvements including removing artefacts (such as pits and spikes) and accounting for coastlines and aquatic bodies [39]. In September 2014, NASA released the third iteration of SRTM3 (also known as "SRTM Plus") for free. It has a 30 m spatial resolution. Compared to the low-resolution SRTM1 (90 m), which only covered regions outside of the US, this version was far more accurate [40]. The dataset might be downloaded from [https://lta.cr.usgs.gov/].

2.3. AW3D-30 DEM

The Panchromatic Remote Sensing Instrument for Stereo Mapping (PRISM) sensor was launched by the Japan Aerospace Exploration Agency (JAXA) on the ALOS (Advanced Land Observing Satellite) satellite in January 2006. A global 5-m (0.15 arcsec) image was generated from approximately 3 million of the 6.5 million photographs that ALOS captured during the mission, which covered a range of latitudes from 80° N to 80° S. The cloud cover was less than 30%. [41]. In 2016, a 30-m resolution version (AW3D30) was made publicly available, which is a resampling of the 5-m version [42]. The dataset could be downloaded from [https://www.eorc.jaxa.jp/ALOS/en/index_e.htm].

2.4. TanDEM-X-90 DEM

The German government launched the high-resolution interferometric SAR (InSAR) radar TanDEM-X (TerraSAR-X add-on for digital elevation measurement) in 2010 through the Aerospace Centre (DLR) in association with EADS Astrium GmbH and Infoterra GmbH (a public-private partnership) consortium [43]. TanDEM-X radar collects Earth data in tandem with TerraSAR-X (launched in June 2007) as a single satellite spacecraft (TerraSARX/ TanDEM-X) in a controlled orbit with a baseline of 250-500 m [42]. The dataset might be downloaded from [http://tandemx-science.dlr.de/].

2.5. Copernicus-30 DEM

A Digital Surface Model (DSM) that faithfully represents the Earth's surface, including buildings, infrastructure, and vegetation, is the Copernicus DEM. With additional characteristics like smoothing water bodies and depicting rivers with regular flow, this DSM is a modified version of WorldDEM. Additionally, some features like airports and improbable terrain formations have been altered, as well as shorelines and coasts. Radar satellite data gathered during the TanDEM-X Mission serves as the foundation for the WorldDEM product. A public-private cooperation between Airbus Defence and Space and the German government, via the German Aerospace Centre (DLR), is funding this project.

OpenTopography provides the global 30m (GLO-30) and 90m (GLO-90) [44]. The following table concludes some characteristics of the four DEM models.

Table 1: DEM Characteristics

DEM	Resolution	Vertical Reference	Description
SRTM3-30	30 m	EGM96	https://lta.cr.usgs.gov/.
AW3D-30	30 m	EGM96	https://www.eorc.jaxa.jp/ALOS/en/index_e.htm
TanDEM-X-90	90 m	WGS84	http://tandemx-science.dlr.de/
Copernicus-30 (COP30)	30 m	EGM2008	OpenTopography - Copernicus GLO-30 Digital Elevation Model

3. Methodology

The experimental studies are in Kom Ombo- Aswan government- Egypt as part of the Future of Egypt for Sustainability national project. This project aims to reclaim around 850,000 acres on Aswan's west bank of the River Nile. Two blocks were surveyed using the GNSS-RTK method to obtain the different levels inside, which helps the designers detect the possible levels for the irrigation pivot systems. The first block has 5090 Acres, and the second has 6985 Acres. Figure 2 shows the map of the two case studies.

3.1. GNSS-RTK solution

A static GPS solution is required to provide a dependable Real-Time Kinematic (RTK) solution. RTK is a technique for improving GPS positioning accuracy that uses data from a fixed reference station, often known as a base station. To do this, a static GNSS station list was created for each block. The stations were observed using Trimble GNSS receivers, based on reference control points belonging to the General Authority for Roads and Bridges (GARB) [45]. These control points were referenced using the global coordinate system (WGS84/UTM zone 36N) and based on EGM2008 as a geoid model. A baseline solution with a GARB reference station has been implemented to resolve the on-site reference station. Continue …*Figure 4* shows the distribution of GARB stations and their relation with the onsite reference stations.

Continue …..*Figure 6.* a refers to the Trimble R4S GNSS receiver as a known base station [GARB], while Continue …..*Figure 6.* b refers to the on-site rover with the Trimble R2 GNSS receiver. In addition, Continue …..*Figure 6.* c shows the 4×4 pickup car used to get the GNSS RTK kinematic DEM data using the Trimble R2 GNSS receiver. The rover was fixed over the vehicle; the moving paths were divided over the area and inserted into the controller. Trimble Business Centre V. 5.2 (TBC v.5.2), which was used to process the static Rinex observations data.

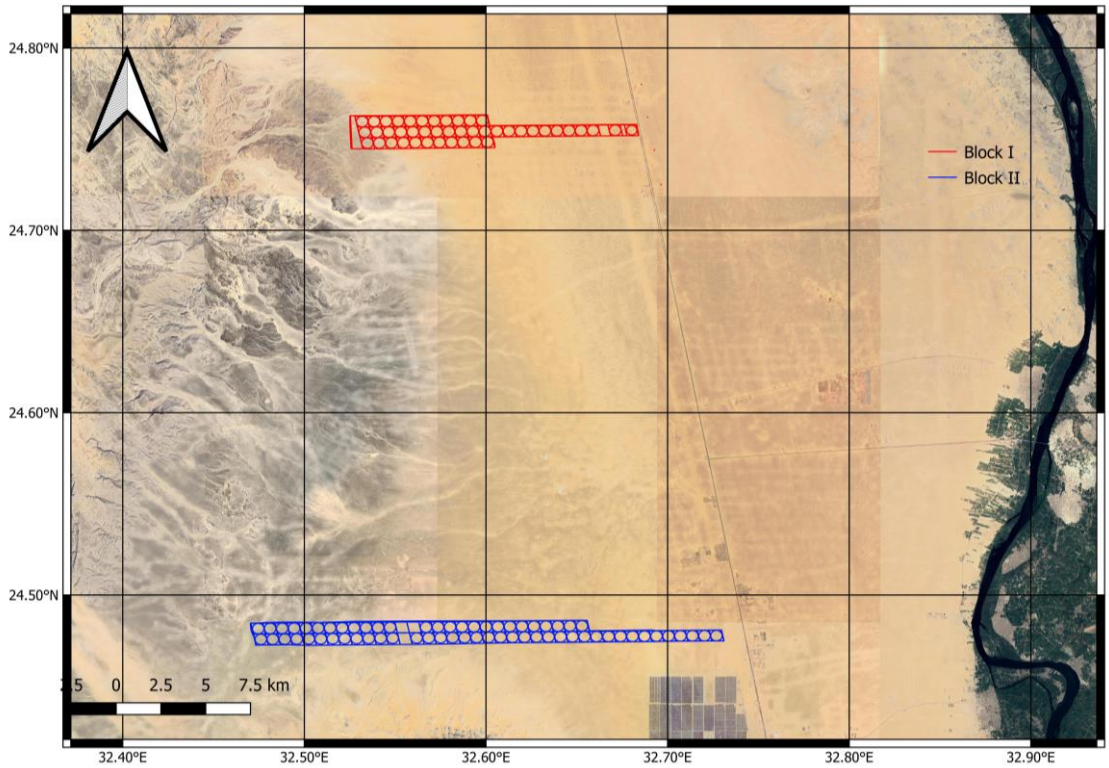

Figure 2: Map of the two case studies, Block I and II

Figure 3: Distribution" of GARB stations and local reference points, the upper image refers to the stations of block I, the lower image for block II

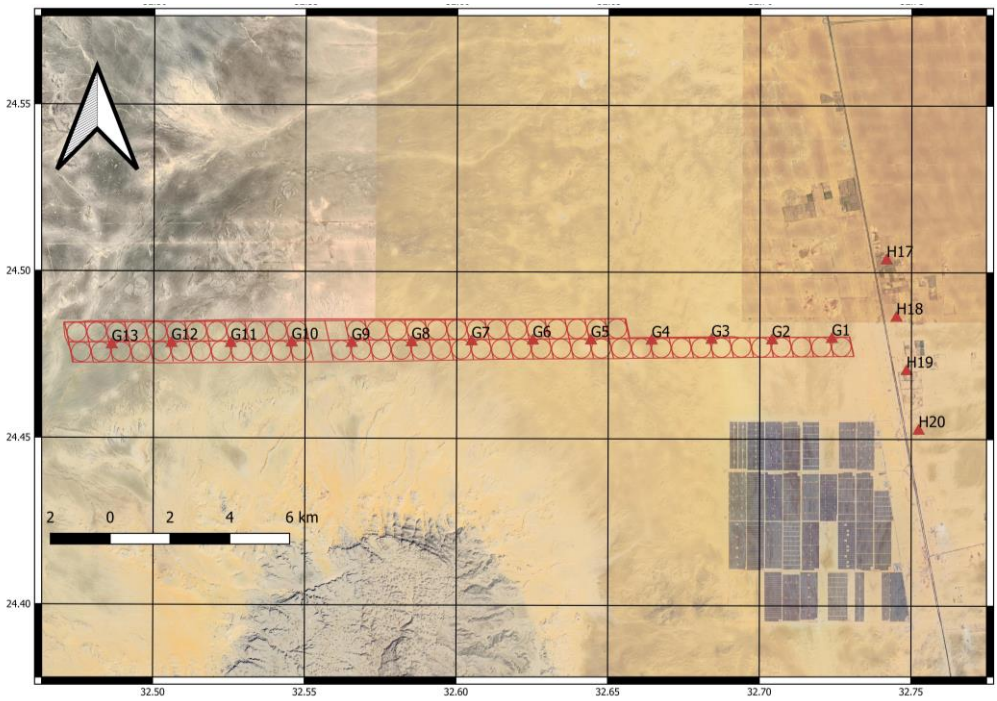

Continue …Figure 4: Distribution" of GARB stations and local reference points, the upper image refers to the stations of block I, the lower image for block II

(a) **(b)**

Figure 5: GNSS receivers over the GARB control points; (a) refers to the base station with Trimble R4S GNSS receiver onsite; (b) refers to the rover station with Trimble R2 GNSS receiver; (c) refers to the GNSS-RTK solution using 4*4 Pickup car

(c)

Continue …..Figure 6: GNSS receivers over the GARB control points; (a) refers to the base station with Trimble R4S GNSS receiver onsite; (b) refers to the rover station with Trimble R2 GNSS receiver; (c) refers to the GNSS-RTK solution using 4*4 Pickup car

The vertical accuracy of any DEM is defined as the discrepancies (d), which refers to the accuracy in the height obtained by the reference height (h_{RTK}) solution and the height derived from the other four DEMs (h_{DEM}) in the study. The discrepancies are expressed as to be seen in Equation (2). According to Equations, the standard deviation (SD), which refers to the deviation relative to the mean value (μ), is estimated in the study. ((3)-(4)). Then, an SD of 95% is estimated by filtering the random errors. To calculate the absolute accuracy of each DEM model, the Root mean square error (*RMSE*) is estimated according to Equation (5).

$$d_i = h_{DEM,\,i} - h_{RTK,i} \tag{2}$$

$$\mu_d = \frac{1}{n}\sum_{i=1}^{n} d_i \tag{3}$$

$$SD_d = \sqrt{\frac{1}{n-1}\sum_{i=1}^{n}(d_i - \mu)^2} \tag{4}$$

$$RMSE_d = \sqrt{\frac{1}{n}\sum_{i=1}^{n}(d_i)^2} \tag{5}$$

Figure 7 Explains the flowchart of the analysis procedure; this flowchart provides five analysis stages. The first stage is the static solution. Stage (2) refers to the RTK solution; this solution is referenced with different geoid models (WGS84- EMG96- EGM2008) according to the reference height for each DEM model. Stage (3) denotes the DEM global

solution and the related height reference. Stage (4) estimates errors according to equation (1). The final step (stage (5)) refers to the statistics estimation (min, mean, max., SD, and RMSE) according to Equations ((2)-(5)).

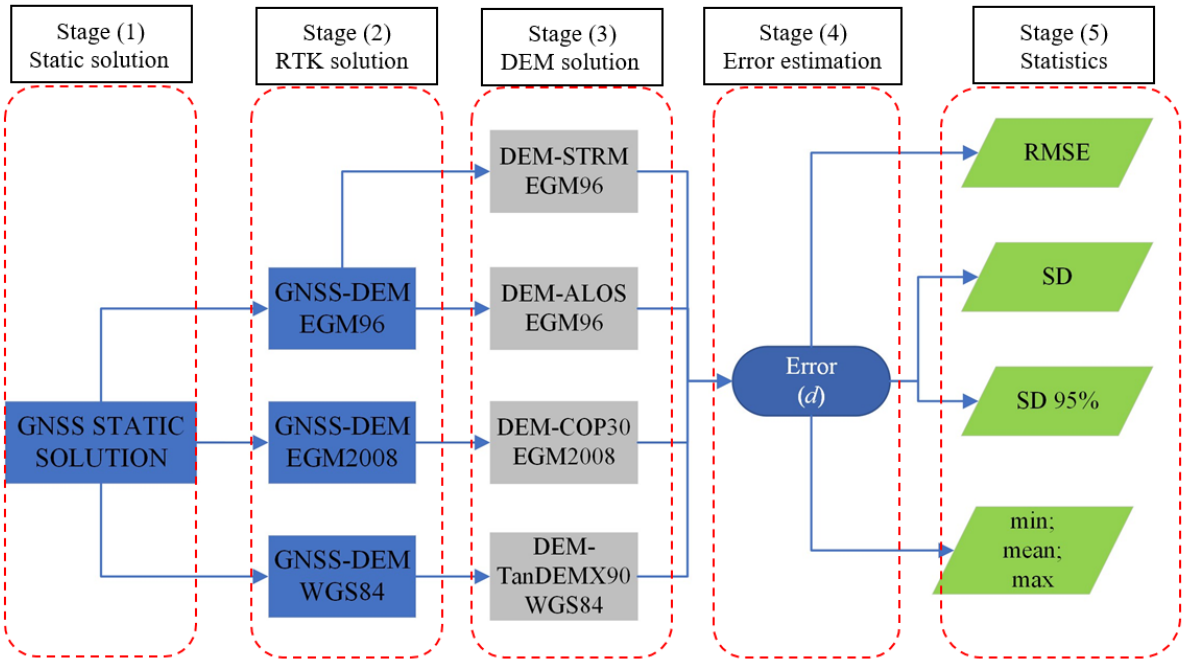

Figure 7: Analysis flowchart

4. Results and discussions

The absolute vertical errors were estimated between the reference height delivered from the GNSS-RTK solution and the global DEM solution obtained from the four examined models for block 1. The distribution of vertical error by DEM is plotted in Figure 8, and the descriptive statistics can be found in Table 2. Table 2 shows the absolute vertical accuracy of STRM 30, ALOS 30, COP 30, and TanDEMX90 models for block 1; the total number of points is (34854) randomly points on-site.

- Model STRM30 exhibits a mean error range of -1.62 meters, encompassing the outliers (-33.16 to 21.27 m). This model shows an RMSE of 3.59 meters and an SD of 3.20 meters; the $SD_{95\%}$ is 2.26 meters after anomalies are eliminated.
- Model ALOS30 shows an error range of (-21.97-15.19 m) with a mean value of -2.8 m and a Root Mean Square Error (RMSE) of 3.30 m. After removing the outliers, the solution initially had a standard deviation of 1.75 m, which decreased to 0.99 m.
- The COP30 model has an error range of -10.83 to -5.42 m, with a mean value of -0.65 m. Moreover, the solution shows a Root Mean Square Error (RMSE) of 0.91 m and a Standard Deviation (SD) of 0.64 m (95% Confidence Interval for SD = 0.43 m).
- The TanDEMX90 model offers the optimal solution, with an error range of -4.22 to 5.11 meters and a mean value of -0.69 meters. The result displayed here has a Root Mean

Square Error (RMSE) of 0.90 and a Standard Deviation (SD) of 0.58 meters, with a 95% confidence interval of 0.38 meters.

Table 2 reveals that both the COP30 model and TanDEX90 model are more accurate than Model STRM30 and Model ALOS30. Model STRM30 and Model ALOS30 have more errors and deviations in the negative direction, where the mean values are (-1.62 m) for model STRM30 and (-2.8 m) for model ALOS30. At the same time, these metrics are greater than those reported by the COP30 model and TanDEX90 model. It should be noted that the COP30 model used a 30 m resolution of pixels for their analysis, while the TanDEX90 model used a 90 m resolution of pixels. The TanDEX90 model has marginally higher accuracy than the COP30 model; it was better. TanDEX90 model has slightly RMSE (0.90 m) and SD (0.58 m) before correlation. In addition, the TanDEX90 model has a relatively more significant R-value (0.9977) than the COP30 model before correlation.

Table 2: Absolute vertical accuracy of STRM30, ALOS30, COP30, and TanDEMX90 models for Block I

DEM	No. of points	RMSE (m)	SD (m)	$SD_{95\%}$ (m)	Min (m)	Mean (μ) (m)	Max (m)	R	$R_{95\%}$
STRM30	34854	3.59	3.20	2.26	-33.16	-1.62	21.27	0.9383	0.9702
ALOS30		3.30	1.75	0.99	-21.97	-2.8	15.19	0.9702	0.9938
COP30		0.91	0.64	0.43	-10.83	-0.65	5.42	0.9938	0.9987
TanDEM-X90		0.90	0.58	0.38	-4.22	-0.69	5.11	0.9977	0.9990

Figure 8 reveals the vertical errors in DEM-STRM and DEM-ALOS 30 have a more normal shape, being unimodal and symmetric. In contrast, DEM-COP 30 and DEM-TanDEMX 90 errors have a strikingly bimodal distribution. The jug nature of the SRTM distribution is likely due to elevation values being given as integers. The density distribution of errors in Figure 8 shows a red colour line (reference (zero) line) and a wider spread of errors for DEM-STRM and DEM-ALOS 30 compared to the COP30 model and TanDEX90 model, where the error distribution was around (6-8) m in the case of DEM-STRM as shown in Figure 8, while the errors decreased gradually (2-4) m for DEM-ALOS 30. This is also evidenced by the Min, Mean, and Max values (for example, the Mean value for the TanDEX90 model was (-0.69) compared to (-1.62) for DEM-STRM). Considering the density distribution of errors and the descriptive statistics computed in Table 2, The TanDEMX90 model is the most accurate compared to all models for block I. The TanDEMX90 model has more verticality and homogenous data, less error, and a more acceptable data shape.

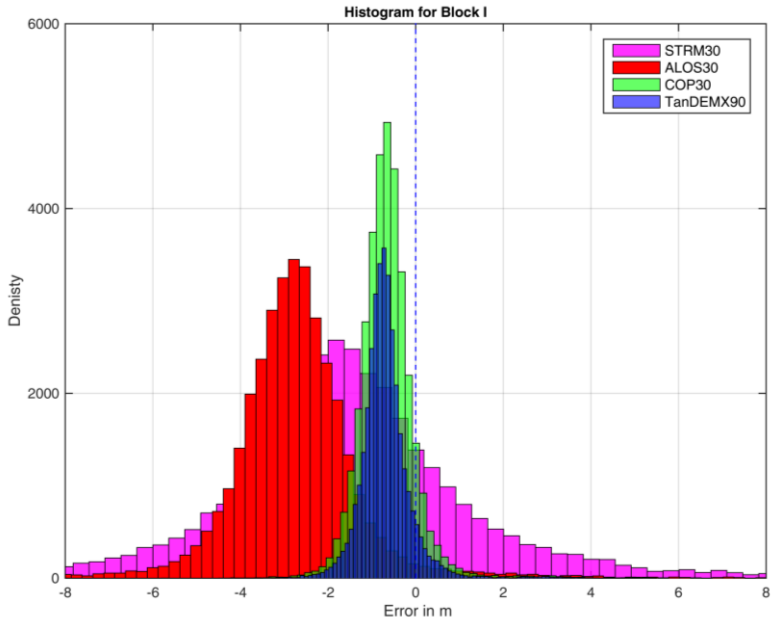

Figure 8: Vertical error distribution for STRM, ALOS 30, COP 30, and TanDEX90 for Block I. The x-axis has been restricted from -8 m to 8 m for visualization; the y-axis is the error distribution

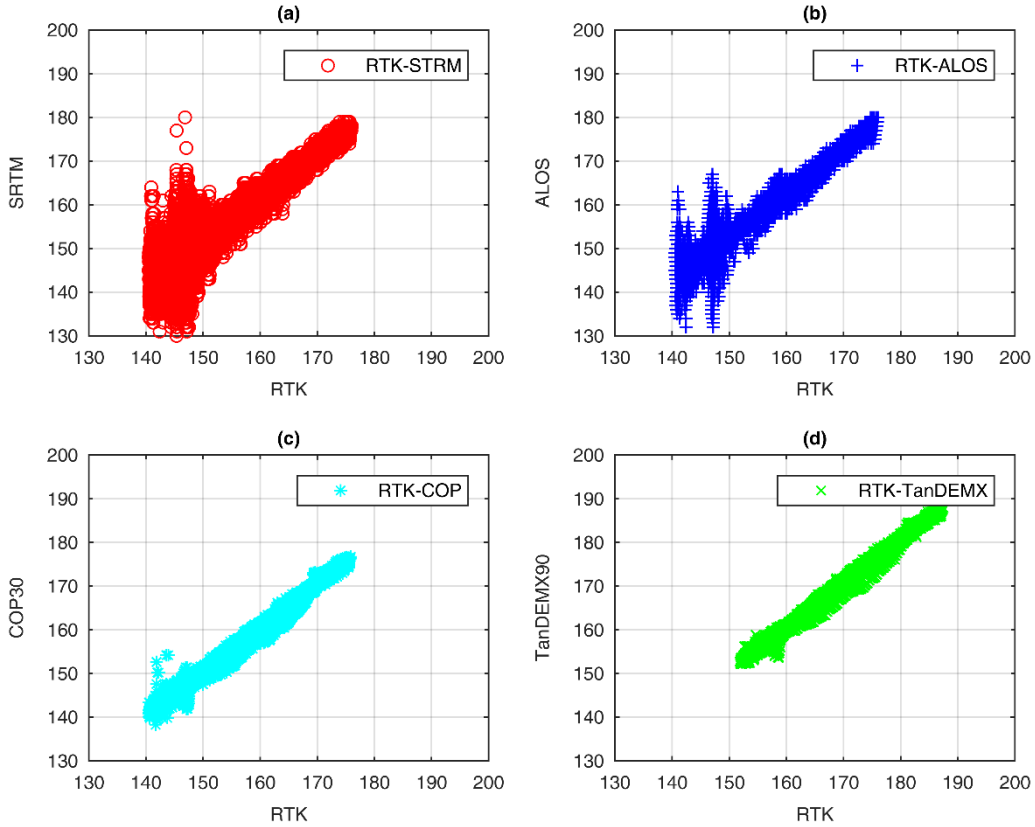

Figure 9: Correlation between levels Using RTK Solution and Z value or Height using STRM 30, ALOS 30, COP 30, and TanDEMX90 models for block I, where the upper four graphs represent the results of correlation without filtering, and the lower four graphs represent the results of correlation with filtering.

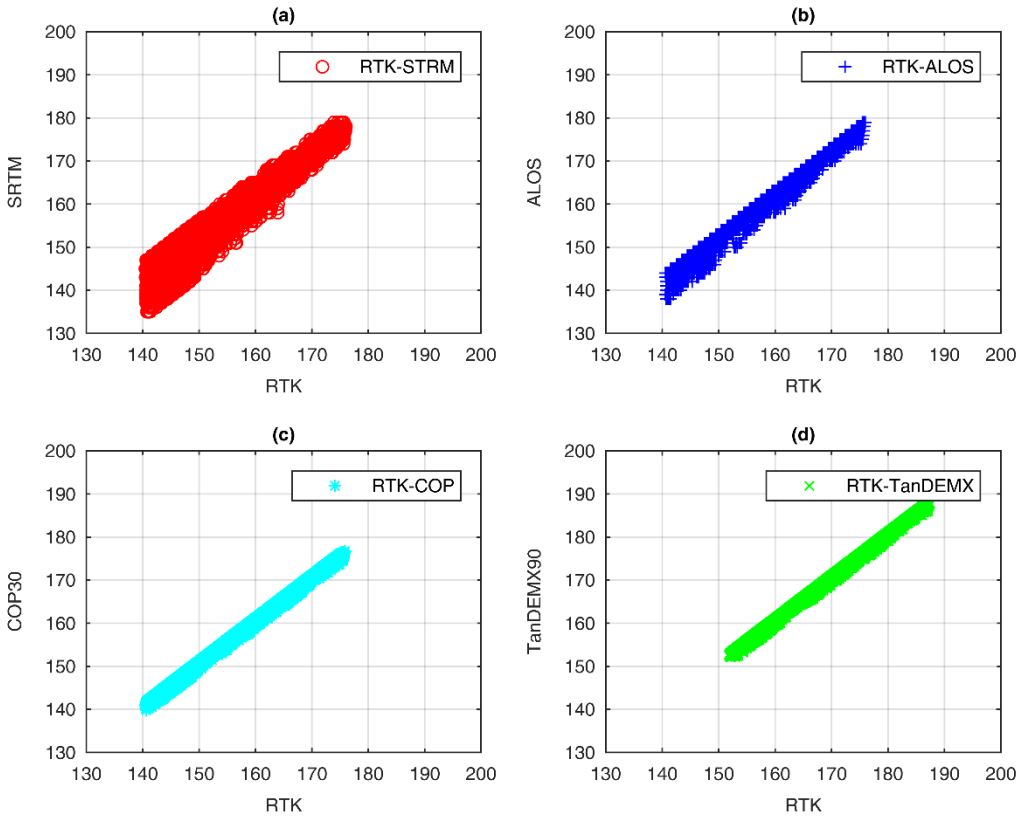

Continue …Figure 10: Correlation between levels Using RTK Solution and Z value or Height using STRM 30, ALOS 30, COP 30, and TanDEMX90 models for block I, where the upper four graphs represent the results of correlation without filtering, and the lower four graphs represent the results of correlation with filtering.

Correlation between levels using RTK and Z or Height for all four models was computed as shown in Continue …Figure 10 below. RMSE is a quadratic metric that puts greater weight on large error values; thus, although the errors in TanDEMX90 are more minor, the more significant errors are distorting the RMSE score despite the use of removing outliers. $R_{95\%}$ and $SD_{95\%}$ (m) were computed using a 5% error assumption to convert the data shape to the standard Gaussian distribution. The results were 43 cm ($SD_{95\%}$ for TanDEMX90) and 38 cm for COP 30. Figure 6 shows the correlation of the relationship shape between the same verticality points for the four models with RTK solution. The X-axis represents levels of points using the RTK solution, and the Y-axis represents the Height for the same point (Z or H). The Y-axis ranges from 130 to 200. If the data were homogenous and had a high degree of similarity, the correlation would be approximately 1.0; otherwise, the correlation would be less than 1.0. The upper four graphs of Continue …Figure 10 show the results of correlation without filtering, whereas the lower four graphs of Figure 6 show the results of correlation after 5% filtering. The results from correlation show that $R_{95\%}$ for TanDEMX90 equals (0.9999), and this value is four models, So TanDEMX90 from German space is the best.

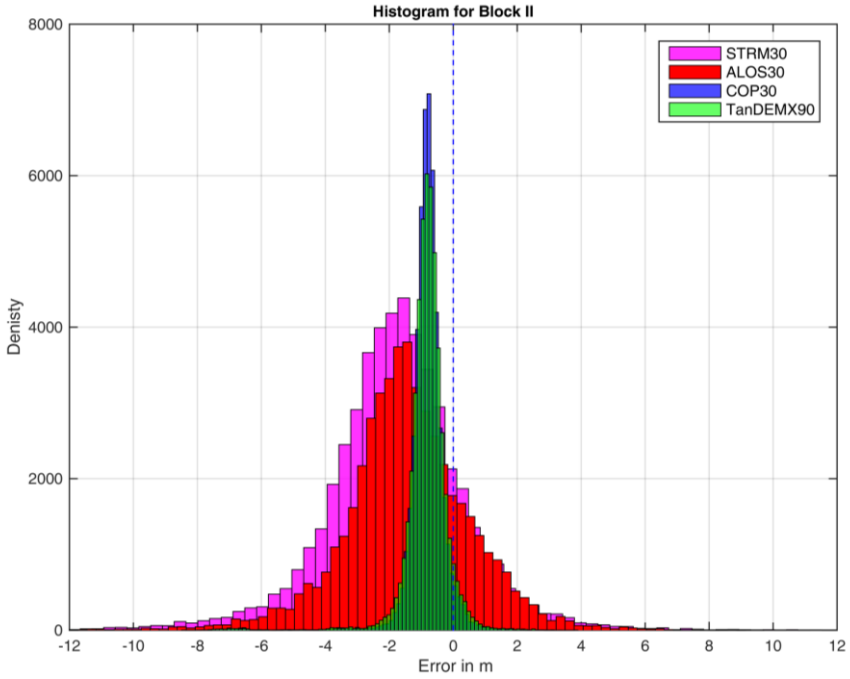

Figure 11: Vertical error distribution for STRM, ALOS 30, COP 30, and TanDEX90 for Block II. The x-axis has been restricted from -8 m to 8 m for visualization; the y-axis is the error distribution.

Table 3: Absolute vertical accuracy of STRM30, ALOS30, COP30, and TanDEMX90 models for Block II

DEM	No. of points	RMSE (m)	SD (m)	$SD_{95\%}$ (m)	Min (m)	Mean (μ) (m)	Max (m)	R	$R_{95\%}$
STRM30	49471	2.92	2.27	1.62	-29.48	-1.83	25.39	0.9721	0.9860
ALOS30		2.58	2.11	1.56	-32.49	-1.47	9.60	0.9774	0.9893
COP30		1.06	0.68	0.40	-8.43	-0.81	3.39	0.9974	0.9991
TanDEM-X90		1.03	0.62	0.34	-7.84	-0.82	3.87	0.9979	0.9993

The same procedure and the estimation of the absolute vertical errors between the reference height solution delivered from the GNSS-RTK solution and the global DEM solution obtained from the four models was done for block II, as shown in Table 3, Figure 11 and Figure 12, respectively. Table 3 shows the total No. of points is (49471) randomly points on-site for Block II, the descriptive statistics display that TanDEMX90 is the most accurate of all (RMSE (1.03 m), SD (0.62 m), Mean (-0.82 m), Min (-7.84 m), Max (3.87 m)).
Figure 11 and Figure 12, respectively, show the density distribution of errors for Block II and the correlation between absolute vertical errors between the reference height solutions delivered from the GNSS-RTK and the global DEM for the four models. The results for Block II are harmonious with those for Block I, where TanDEX90 was the most accurate for Block II and R95% for Block II (0.9993 m). This means that TanDEX90 has more verticality and homogenous data and less error for both Block I and II.

5. Machine Learning Analysis

Recently, many efforts have been made to improve the quality and quantity of detected and identified coordinate points on specific blocks on Earth depending on satellite systems. These extracted and obtained data from different DEM solutions need validation by comparing and matching them to the extracted images from GPS regarding coordination systems, boundaries, and essential points on the specific blocks on Earth [46]. As many methods were proposed and performed, such as DEM solutions in this field, machine learning came to validate these methods and identify the most accurate solutions to be considered and recommended in future directions of the survey field studies [47]. In this research, the Support Vector Machine Model (SVM) was used to measure the ability of the selected DEM solutions to detect the exact coordination system of the extracted images from the satellite system using GNSS-RTK for the two different blocks in Egypt. SVM is a binary detection model that uses two categories of high-dimensional data sets to predict the performance of the input parameters. It is initially used to solve and work with classification problems with binary aspects (0,1) [48].

The performance of the previously mentioned methods was analysed using a machine learning model named Support Vector Machine, and the performance of each selected method was studied and tested separately according to the model in a binary comparison. The GNSS-RTK data was obtained from a GNSS system and considered significant, actual values to be used for measuring the validation of other methods in conducting the satellite data. Therefore, the research focused on measuring each selected method's efficiency and ability to determine the boundaries and choose regular points of two-block samples of land plots in inaccurate ways.

Four DEM solutions were considered in the selected machine learning model, including STRM-EGM96, ALOS-EGM96, COP30-EGM2008, and TanDEMX90-WGS84. The proper reference DEM solution was chosen, which GNSS-RTK is. The dataset was divided into testing and training sets at 30:70 for each SVM model development. Different sample sizes were trained using the selected machine learning model to be used later for testing the rest of the obtained data, with about 10,400 readings from sample 1 and about 10,000 from sample 2, as seen in Table 4 and Table 5 , respectively. The Tables show the efficiency of the four DEM solutions in detecting the correct points on the selected blocks. The SVM model was built and developed on MATLAB software with a prepared code for prediction purposes. Firstly, the trained data were labelled into groups according to the DEM methods, and then every group was trained separately to identify the results of detecting the blocks with fewer mistakes. 70% of the data were trained at the same procedures to provide the full ability to the model to select the best choice of the DEM method. Later, the full data (training and testing) datasets were combined and tested at the same level of comfort to show the most effective DEM solution that can be used for agricultural purposes. The

Tables show the efficiency of the four DEM solutions in detecting the correct points on the selected blocks.

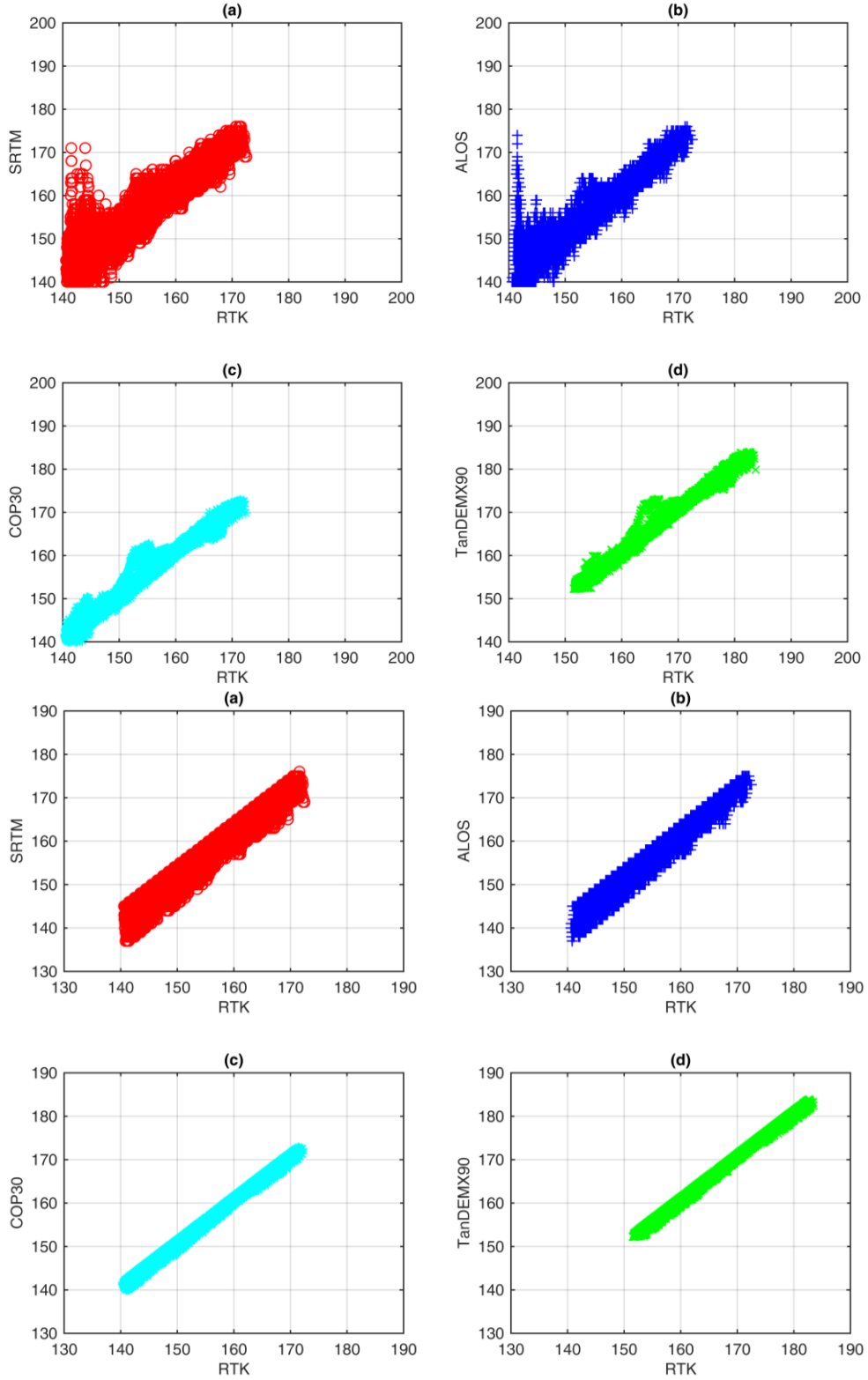

Figure 12: Correlation between levels Using RTK Solution and Z value or Height using STRM 30, ALOS 30, COP 30, and TanDEMX90 models for block II; where the upper side represents the results of correlation without filtering and the lower side represents the results of correlation with filtering.

Table 4: The performance of the selected DEM solution in detecting the points on Block 1

DEM Solution	Precision	Recall	F1-Score	Support	Accuracy
GNSS-RTK	0.999	1.000	0.999	34,855	0.98
STRM30	0.848	0.498	0.627	10,400	0.838823
ALOS30	0.817	0.532	0.644	10,400	0.830401
COP30	0.834	0.573	0.679	10,400	0.839002
TanDEM-X90	0.851	0.208	0.334	10,400	0.846778

Table 4 shows the efficiency of using the selected four DEM solutions in identifying and determining the proper and correct (x, y, and z) values from Block I. The results are relatively close to each other. More clearly, the results show that the accuracy of detecting the points on Block I using the DEM-TanDEMX90-WGS84 was significant and achieved higher accuracy values than the other selected DEM solutions, with about 84.7%. Also, the results reveal that the recall values are relatively low, and the different metrics, like precision and f1-score values, show relatively high values.

In addition, the COP30-EGM2008 solution results show a high accuracy value of about 83.8%. The accuracy results of the STRM-EGM96 and ALOS-EGM96 are relatively low compared to the TanDEMX90-WGS84 results, with about 83.8% and 83%, respectively. Moreover, the metric values of the model, including precision, recall, and f1-score, show the ability of the selected DEM solution to detect and identify the correct points that match the GNSS-RTK solution values for Block I.

In Table 5, the results show that the selected DEM solution, called TanDEMX90 WGS84, is significant in detecting and identifying the points on Block II that match data obtained from the GNSS-RTK solution, with an accuracy of about 85.3%. In contrast, the lower accuracy value at about 83% is achieved by using the STRM-EGM96. Also, the other DEM solutions show acceptable and high accuracy values, with about 85% for the COP30-EGM2008 and 83.1% for the ALOS-EGM96. This relatively low accuracy variance between the two previously selected DEM solutions reveals the significance of these methods for further studies that aim to detect and determine the valid points of blocks on Earth.

Table 5: The performance of the selected DEM solution in detecting the points on Block II

DEM Solution	Precision	Recall	F1-Score	Support	Accuracy
GNSS-RTK	0.999	1.000	0.9995	49,472	0.98
STRM30	0.800	0.449	0.575447	10,000	0.830481
ALOS30	0.819	0.591	0.686686	10,000	0.831330
COP30	0.793	0.599	0.682547	10,000	0.849797
TanDEM-X90	0.820	0.403	0.540578	10,000	0.852941

6. Conclusions

With the huge developments in agriculture in the Egypt sector, this paper evaluates the free DEM models' accuracy compared to the GNSS-RTK solution. Four DEM models have been evaluated [STRM30, ALOS30, COP30, and TanDEM-X90]. The experimental research is being conducted in Kom Ombo, Aswan, Egypt, as part of the National Future of Egypt for Sustainability project. This project intends to reclaim around 850,000 acres along Aswan's west bank of the Nile. Two blocks were surveyed using the GNSS-RTK approach to determine the various levels inside, allowing the designers to identify potential levels for irrigation pivot systems. The first block has 5090 acres, while the second has 6985 acres. Based on the literature review and case study. The suitability of a free DEM for agricultural applications in nearly flat topography is determined by several factors, including the resolution of the DEMs and the accuracy of the free DEM, which can result in incorrect assessments of land suitability, drainage patterns, and other agricultural planning needs. The results are connected to its case study for the near flat region, and the delivered precision may be useful for the pre-study of reclamation areas, as well as the primary pattern of the irrigation process and the pre-estimation of earthwork volumes on site.

The following are the conclusions of the research paper:

- The reference data for the evaluation is a GNSS-RTK solution with Static-GNSS control points to strengthen the reliability of the results.
- Model STRM30 delivered the worst solution with an RMSE of 3.59 m and 2.92 m for Block I and II, respectively.
- The ALOS30 model comes third according to accuracy, which reported an RMSE of 3.30 m for block I and 2.58 m for block II.
- Model COP30 is the second one with an RMSE value of .91 m and a value of 1.06 m for blocks I and II.
- The most accurate model from this study is TanDEM-X90, which offered an RMSE of 0.90 m for block I with an SD of 0.58 m ($SD_{95\%}$ = 0.38 m). Regarding block II, the model reported an RMSE of 1.03 m with an SD value of 0.62 m, and after eliminating the anomalies, was 0.34 m. This result is very optimistic, suggesting that the high resolution from this model might improve the DEM results significantly compared to the truth values using the GNSS-RTK solution.
- By using the machine learning techniques, the classification showed that as well as the classical comparison, TanDEM-X90 is the best solution with an accuracy of 84.7% for block I and 85% for block II.

References

[1] Rahmati, O., Yousefi, S., Kalantari, Z., Uuemaa, E., Teimurian, T., Keesstra, S., Pham, T. D. and Tien Bui, D. (2019). Multi-Hazard Exposure Mapping Using Machine Learning Techniques: A Case Study From Iran. *Remote Sensing,* 11**,** 1943.

[2] Scown, M. W., Thoms, M. C. and De Jager, N. R. (2015). Floodplain Complexity and Surface Metrics: Influences Of Scale And Geomorphology. *Geomorphology,* 245**,** 102-116.

[3] Bonilla-Sierra, V., Scholtes, L., Donzé, F. & Elmouttie, M. (2015). Rock Slope Stability Analysis Using Photogrammetric Data And DFN–Dem Modelling. *Acta Geotechnica,* 10**,** 497-511.

[4] Fenta, A. A., Kifle, A., Gebreyohannes, T. and Hailu, G. (2015). Spatial Analysis Of Groundwater Potential Using Remote Sensing And GIS-Based Multi-Criteria Evaluation in Raya Valley, Northern Ethiopia. *Hydrogeology Journal,* 23**,** 195.

[5] He, Y., Song, Z. and Liu, Z. (2017). Updating Highway Asset Inventory Using Airborne Lidar. *Measurement,* 104**,** 132-141.

[6] Zhang, K., Gann, D., Ross, M., Robertson, Q., Sarmiento, J., Santana, S., Rhome, J. and Fritz, C. (2019). Accuracy Assessment Of ASTER, SRTM, ALOS, AND TDX DEMS For Hispaniola and Implications for Mapping Vulnerability to Coastal Flooding. *Remote Sensing of Environment,* 225**,** 290-306.

[7] Li, L., Nearing, M. A., Nichols, M. H., Polyakov, V. O., Guertin, D. P. and Cavanaugh, M. L. (2020). The Effects Of Dem Interpolation on Quantifying Soil Surface Roughness Using Terrestrial Lidar. *Soil And Tillage Research,* 198**,** 104520.

[8] Heo, J., Jung, J., Kim, B. and Han, S. (2020). Digital Elevation Model-Based Convolutional Neural Network Modeling for Searching Of High Solar Energy Regions. *Applied Energy,* 262**,** 114588.

[9] Bhatta, B., Shrestha, S., Shrestha, P. K. and Talchabhadel, R. (2019). Evaluation and Application of A SWAT Model To Assess The Climate Change Impact On The Hydrology Of The Himalayan River Basin. *Catena,* 181**,** 104082.

[10] Amirkolaee, H. A., Arefi, H., Ahmadlou, M. and Raikwar, V. (2022). Dtm Extraction from DSM Using A Multi-Scale Dtm Fusion Strategy Based On Deep Learning. *Remote Sensing Of Environment,* 274**,** 113014.

[11] Maune, D. F., Kopp, S. and Zerdas, C. (2007). Digital Elevation Model Technologies And Applications. *The Dem Users Manual*.

[12] Pavlis, N. K., Holmes, S. A., Kenyon, S. C. & Factor, J. K. (2012). The Development And Evaluation of The Earth Gravitational Model 2008 (Egm2008). *Journal Of Geophysical Research: Solid Earth,* 117.

[13] Milbert, D. G. and Smith, D. A. Converting GPS Height into NAVD88 Elevation with the GEOID96 Geoid Height Model. (1996). *GIS LIS-International Conference,* 681-692.

[14] Leick, A., Rapoport, L. and Tatarnikov, D. (2015). *GPS Satellite Surveying,* John Wiley & Sons.

[15] Farah, A., Talaat, A. and Farrag, F. (2008). Accuracy Assessment Of Digital Elevation Models Using GPS. *Artificial Satellites,* 43, 151-161.

[16] Abdallah, A., Saifeldin, A., Abomariam, A. and Ali, R. (2020). Efficiency of Using GNSS-PPP for Digital Elevation Model (DEM) Production. *Artificial Satellites,* 55, 17-28.

[17] Abdallah, A. (2016). Precise Point Positioning For Kinematic Applications to Improve Hydrographic Survey. " Ph.D. dissertation, Univ. of Stuttgart, Stuttgart, Germany.

[18] Hofmann-Wellenhof, B., Lichtenegger, H. and Wasle, E. (2007). GNSS–Global Navigation Satellite Systems: GPS, GLONASS, GALILEO, and More, *Springer Science & Business Media*.

[19] Li, J., Chapman, M. and Sun, X. (2006). Validation of Satellite-Derived Digital Elevation Models From In-Track Ikonos Stereo Imagery. *Ontario Ministry Of Transport*, Toronto.

[20] Fisher, P. F. and Tate, N. J. (2006). Causes And Consequences of Error in Digital Elevation Models. *Progress In Physical Geography,* 30, 467-489.

[21] Hebeler, F. and Purves, R. S. (2009). The Influence Of Elevation Uncertainty on Derivation of Topographic Indices. *Geomorphology*, 111, 4-16.

[22] Van Zyl, J. J. (2001). The Shuttle Radar Topography Mission (SRTM): A Breakthrough In Remote Sensing of Topography. *Acta Astronautica*, 48**,** 559-565.

[23] Werner, M. (2001). Shuttle Radar Topography Mission (SRTM) Mission Overview. *Frequenz*, 55, 75-79.

[24] Takaku, J., Tadono, T., Doutsu, M., Ohgushi, F. and Kai, H. (2020). Updates Of 'Aw3d30'alos Global Digital Surface Model with Other Open Access Datasets. *The International Archives Of The Photogrammetry, Remote Sensing And Spatial Information Sciences*, 43, 183-189.

[25] Rizzoli, P., Martone, M., Gonzalez, C., Wecklich, C., Tridon, D. B., Bräutigam, B., Bachmann, M., Schulze, D., Fritz, T. and Huber, M. (2017). Generation and Performance Assessment of the Global TANDEM-X Digital Elevation Model. *ISPRS Journal Of Photogrammetry And Remote Sensing*, 132, 119-139.

[26] Uuemaa, E., Ahi, S., Montibeller, B., Muru, M. and Kmoch, A. (2020). Vertical Accuracy of Freely Available Global Digital Elevation Models (ASTER, AW3D30, MERIT, TANDEM-X, SRTM, And NASADEM). *Remote Sensing*, 12, 3482.

[27] Pakoksung, K. and Takagi, M. (2021). Assessment And Comparison of Digital Elevation Model (Dem) Products in Varying Topographic, Land Cover Regions and Its Attribute: A Case Study In Shikoku Island Japan. *Modeling Earth Systems And Environment*, 7, 465-484.

[28] Hawker, L., Neal, J. and Bates, P. (2019). Accuracy Assessment of the TANDEM-X 90 Digital Elevation Model for Selected Floodplain Sites. *Remote Sensing Of Environment*, 232, 111319.

[29] Preety, K., Prasad, A. K., Varma, A. K. and El-Askary, H. (2022). Accuracy Assessment, Comparative Performance, And Enhancement of Public Domain Digital Elevation Models (ASTER 30 m, SRTM 30 m, CARTOSAT 30 m, SRTM 90 m, MERIT 90 m, and TANDEM-X 90 m) using DGPS. *Remote Sensing*, 14**,** 1334.

[30] Jain, A. O., Thaker, T., Chaurasia, A., Patel, P. and Singh, A. K. (2018). Vertical Accuracy Evaluation Of SRTM-Gl1, GDEM-V2, AW3D30 And CARTODEM-V3. 1 of 30-m Resolution with Dual Frequency GNSS For Lower Tapi Basin India. *Geocarto International*, 33, 1237-1256.

[31] Marešová, J., Gdulová, K., Pracná, P., Moravec, D., Gábor, L., Prošek, J., Barták, V. and Moudrý, V. (2021). Applicability Of Data Acquisition Characteristics to the Identification Of Local Artefacts in Global Digital Elevation Models: Comparison of The COPERNICUS And TANDEM-X Dems. *Remote Sensing*, 13, 3931.

[32] El Ashiry, A. and Elkhalil, O. (2024). Vertical Accuracy Assessment for The Free Digital Elevation Models SRTM and ASTER in Various Sloping Areas. *Jes. Journal Of Engineering Sciences*, 52, 250-268.

[33] Polidori, L. and El Hage, M. (2020). Digital Elevation Model Quality Assessment Methods: A Critical Review. *Remote Sensing*, 12, 3522.

[34] Fazilova, D., Magdiev, K. and Sichugova, L. (2021). Vertical Accuracy Assessment of Open Access Digital Elevation Models Using GPS. *International Journal of Geoinformatics*, 17, 19-26.

[35] Ferreira, Z. A. and Cabral, P. (2022). A Comparative Study about Vertical Accuracy Of Four Freely Available Digital Elevation Models: A Case Study In The Balsas River Watershed, Brazil. *ISPRS International Journal of Geo-Information*, 11, 106.

[36] Cai, C. and Gao, Y. (2013). Modeling And Assessment of Combined GPS/GLONASS Precise Point Positioning. *GPS Solutions*, 17, 223-236.

[37] Szypuła, B. (2019). Quality Assessment of DEM Derived From Topographic Maps for Geomorphometric Purposes. *Open Geosciences*, 11, 843-865.

[38] Mashimbye, Z. E., De Clercq, W. P. and Van Niekerk, A. (2014). An Evaluation of Digital Elevation Models (DEMS) for Delineating Land Components. *Geoderma*, 213, 312-319.

[39] DAAC, L. (2015). The Shuttle Radar Topography Mission (SRTM) Collection User Guide. NASA EOSDIS Land Processes DAAC, USGS Earth Resources Observation and Science (EROS) Center: Sioux Falls, Sd, Usa.

[40] Rabah, M., El-Hattab, A. and Abdallah, M. (2017). Assessment Of The Most Recent Satellite Based Digital Elevation Models of Egypt. *NRIAG J Astron Geophys*.

[41] ALOSWORLD3D. (2023). *Alos World 3d* [Online]. Available: Https://Portal.Opentopography.Org/Raster?Opentopoid=Otalos.112016.4326.2 [Accessed 22.12.2023].

[42] Grohmann, C. H. (2018). Evaluation of Tandem-X Dems on Selected Brazilian Sites: Comparison with SRTM, ASTER GDEM and ALOS AW3D30. *Remote Sensing of Environment,* 212**,** 121-133.

[43] DLR-TANDEM-X. (2023). *DLR-TANDEM-X* [Online]. Available: Https://Www.Dlr.De/Hr/En/Desktopdefault.Aspx/Tabid-2317/3669_Read-5488/ [Accessed 22-12-2023].

[44] COPERNICUS (2024). Copernicus Global Digital Elevation Models.

[45] GARB. (2024). *GARB* [Online]. Available: [https://garb.gov.eg/] [Accessed 6 2024].

[46] Habib, A., Akdim, N., El Ghandour, F.-E., Labbassi, K., Khoshelham, K. and Menenti, M. (2017) Extraction and Accuracy Assessment of High-Resolution Dem and Derived Orthoimages from ALOS-PRISM Data over Sahel-Doukkala (Morocco). *Earth Science Informatics,* 10**,** 197-217.

[47] Biswal, S., Sahoo, B., Jha, M. K. and Bhuyan, M. K. (2023). A Hybrid Machine Learning-Based Multi-Dem Ensemble Model Of River Cross-Section Extraction: Implications on Streamflow Routing. *Journal of Hydrology,* 625**,** 129951.

[48] Ziari, H., Maghrebi, M., Ayoubinejad, J. and Waller, S. T. (2016). Prediction of Pavement Performance: Application Of Support Vector Regression With Different Kernels. *Transportation Research Record,* 2589**,** 135-145.